inorganics

MDPI

Article

A Computational Chemistry Investigation of the Influence of Steric Bulk of Dithiocarbamato-Bound Organic Substituents upon Spodium Bonding in Three Homoleptic Mercury(II) Bis(N,N-dialkyldithiocarbamato) Compounds for Alkyl = Ethyl, Isobutyl, and Cyclohexyl

Rosa M. Gomila, Edward R. T. Tiekink * and Antonio Frontera *

Department of Chemistry, Universitat de les Illes Balears, Crta de Valldemossa km 7.5, 07122 Palma de Mallorca, Spain; rosa.gomila@uib.es

* Correspondence: edward.tiekink@gmail.com (E.R.T.T.); toni.frontera@uib.es (A.F.)

Abstract: Three homoleptic $Hg(S_2CNR_2)_2$, for R = ethyl (**1**), isobutyl (**2**), and cyclohexyl (**3**), compounds apparently exhibit a steric-dependent supramolecular association in their crystals. The small group in **1** allows for dimer formation via covalent Hg–S interactions through an eight-membered $\{–HgSCS\}_2$ ring as the dithiocarbamato ligands bridge centrosymmetrically related Hg atoms; intradimer Hg···S interactions are noted. By contrast, centrosymmetrically related molecules in **2** are aligned to enable intermolecular Hg···S interactions, but the separations greatly exceed the van der Waals radii. The large group in **3** precludes both dimerization and intermolecular Hg···S interactions. Computational chemistry indicates that the potential region at the Hg atom is highly dependent on the coordination geometry about the Hg atom. Intramolecular (**1**) and intermolecular (**2**) spodium bonding (SpB) is demonstrated. Even at separations approaching 0.4 Å beyond the sum of the assumed van der Waals radii, the energy of the stabilization afforded by the structure directs SpB in **2** amounts to approximately 2.5 kcal/mol. A natural bond orbital (NBO) analysis points to the importance of the LP(S) → σ*(Hg–S) charge transfer and to the dominance of the dispersion forces and electron correlation to the SpB in **2**.

Keywords: mercury; dithiocarbamate; steric effects; noncovalent interactions; spodium bonding; molecular electrostatic potential (MEP); quantum theory of atoms in molecules (QTAIM); noncovalent interaction plots (NCIPLOT); interaction energy; molecular orbitals

Citation: Gomila, R.M.; Tiekink, E.R.T.; Frontera, A. A Computational Chemistry Investigation of the Influence of Steric Bulk of Dithiocarbamato-Bound Organic Substituents upon Spodium Bonding in Three Homoleptic Mercury(II) Bis(N,N-dialkyldithiocarbamato) Compounds for Alkyl = Ethyl, Isobutyl, and Cyclohexyl. *Inorganics* **2023**, *11*, 468. https://doi.org/10.3390/inorganics11120468

Academic Editor: Michael A. Beckett

Received: 19 October 2023
Revised: 27 November 2023
Accepted: 29 November 2023
Published: 1 December 2023

1. Introduction

The complexation of heavy elements, for example, d- and p-block elements, by dithiocarbamato ligands has long been a mainstay of coordination chemistry as these are very effective chelators [1–6], see Figure 1 for a generic chemical diagram for a monofunctional dithiocarbamato ligand. Among these compounds, those of the zinc triad elements have long attracted the attention of structural chemists owing to the fascinating range of molecular structures in their crystals [7–10]. A crucial factor for the observed diverse range of structural motifs is the ability of Zn, Cd, and Hg to extend their coordination spheres through secondary bonding interactions. The term "secondary bonding" is generic [11] and was initially employed to cover a myriad of long-recognized intermolecular contacts operating between molecules in various phases [12–14], but is now usually replaced by more specific terms reflecting the nature of the supramolecular aggregation for a particular Group of the Periodic Table [15–18]. In the case of the zinc triad elements, the term "spodium bonding" applies [19]. This term is widely adopted, as revealed in subsequent systematic and computational chemistry studies [20–28], and, along with other Periodic Table Group-specific intermolecular interactions based on the σ-hole and π-hole

concepts [29–34], spodium bonding is expected to be most prominent for the heavier Group 12 element, mercury.

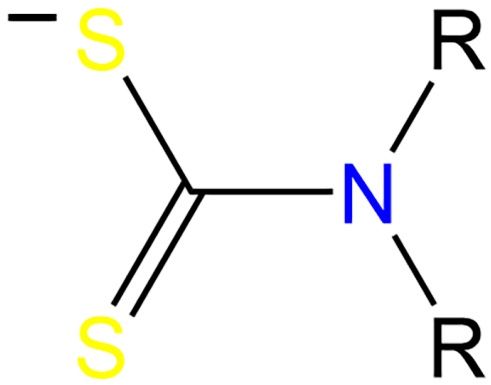

Figure 1. Chemical diagram for one canonical form of a generic dialkyldithiocarbamato anion.

Owing to the presence of two S atoms per dithiocarbamato anion and the inherent thiophilic character of Hg, the presence of Hg···S interactions in crystals of mercury(II) dithiocarbamato compounds might very well be anticipated. Certainly, in crystals of the homoleptic $Hg(S_2CNRR')_2$ compounds, for R, R′ = H, alkyl or aryl, Hg···S interactions are often observed [35]. A factor mitigating intermolecular Hg···S interactions and analogous secondary bonding interactions in crystals of p-block dithiocarbamato compounds, and those of related xanthato ($^{-}S_2COR$) and dithiophosphato [$^{-}S_2P(OR)(OR')$] compounds, are steric effects exerted by the 1,1-dithiolato-bound organic substituents and/or heavy element-bound organic substituents in the case of organometallic species [7–10,36,37].

In the above context and in continuation of recent systematic investigations of supram olecular aggregation patterns based on Hg···S interactions in organomercury [38] and non organomercury crystals [39], the present study describes a computational chemistry investigation of three homoleptic $Hg(S_2CNR_2)_2$ compounds, for R = ethyl (**1**) [40,41], isobutyl (**2**) [42], and cyclohexyl (**3**) [43]. These literature structures are notable in that through the agency of bidentate, bridging dithiocarbamato ligands, and strong intermolecular Hg–S interactions in **1**, a dimeric aggregate is formed. Dimers are not evident in **2** even though the molecules are aligned to potentially dimerize; instead, weak intermolecular Hg···S interactions are apparent between these molecules. In **3**, no evidence for intermolecular Hg···S interactions is found. One interpretation of this variation rests with the reduced propensity of the molecules to dimerize as the steric bulk of the remote nitrogen-bound substituent increases. It should also be noted here that the electronic structure of the dithiocarbamato anion is not influenced in any significant fashion by the nature of the nitrogen-bound substituent, as evidenced in the very small spreads of the Ni–S bond lengths in the uniformly square planar homoleptic $Ni(S_2CNRR')_2$ complexes [4] and of the Te–S bond lengths in the uniformly trapezoidal planar, homoleptic $Te(S_2CNRR')_2$ compounds [5]. In this study, the respective aggregates (**1** and **2**) and molecule (**3**) have been analyzed by a variety of computational chemistry techniques like the molecular electrostatic potential (MEP), the quantum theory of atoms in molecules (QTAIM), noncovalent interaction plots (NCIPLOT), the energetics of the relevant interactions calculated, and assessments of molecular orbitals to determine the nature of the intermolecular binding between molecules in the crystals of **1**–**3**.

2. Methods

Crystallographic data employed in the present study were extracted as Crystallographic Information Files (CIFs) from the Cambridge Structural Database (CSD; [44]); the CIF employed for **1** was of a redetermination based on single crystal data [41]. Crystallographic analyses were conducted by employing a combination of PLATON [45] and MoloVol 1.1.1.0 [46]. Crystallographic diagrams were generated with DIAMOND 3.2.11.0 [47].

The comparative Hirshfeld analysis was conducted with CrystalExplorer21 [48] in accord with established protocols [49].

The evaluation of the salient interactions found in the respective crystals through computational chemistry calculations was achieved using the program Turbomole 7.7 [50] with the input coordinates being those derived from previous crystallographic studies, as available in the respective CIFs [41–43]. The two conformations of **1** were fully optimized without symmetry constraints. The level of theory employed for the calculations was PBE0-D4/def2-TZVP [51–54]. For Hg, this basis set includes the effective core potential (ECP) and for the inner electrons, allows for relativistic effects [53]. The same level of theory with 0.001 a.u. isosurfaces provided wavefunctions enabling the generation of the MEP surface plots. The Bader quantum theory of atoms in molecules (QTAIM) method [55] was used for the topological analysis of the electron density with the reduced density gradient (RDG) isosurfaces (NCI plots) [56] generated by the VMD program 1.9.4 [57]. The Natural Bond Orbital (NBO) analysis [58] was performed using the level of theory as above through the NBO7.0 program [59]. The NBOs and spin density plots were represented using the VMD software 1.9.4 [57]. The energy decomposition analysis (EDA) analysis was performed using the Kitaura–Morokuma method [60], as implemented in Turbomole 7.7 [50]. The QTAIM parameters for the complexes analyzed herein are summarized in Table S1 and the Cartesian coordinates are given in Table S2 (Supplementary Information File).

3. Results and Discussion

Initially, an overview of the structural motifs found for $Hg(S_2CNRR')_2$ in the solid state, as determined by X-ray crystallography, is presented. Then, a detailed description of the molecular geometries of **1**–**3**, the focus of the present study, is given along with an assessment of Hg···S interactions operating in their respective crystals (Section 3.2). The overview is followed by a detailed analysis of the nature of the bonding between molecules in **1**–**3** through computational chemistry techniques (Section 3.3).

3.1. Literature Survey

As indicated in the Introduction, X-ray crystallography on mercury(II) dithiocarbamato compounds, more specifically, molecules conforming to the general formula $Hg(S_2CNRR')_2$, that is, with a single CS_2 residue per dithiocarbamate ligand, exhibits an assorted array of molecular and supramolecular assemblies. Such structural diversity is far from being restricted to mercury(II) dithiocarbamato structures as mercury compounds, including organomercury species, are historically well known to adopt varying structural motifs in their crystals [61–64], partly arising from their ability to form mercurophilic interactions [65]. Since the last detailed overview of $Hg(S_2CNRR')_2$ structures about a decade ago [35], the number of the literature examples has grown by well over 50%, reflecting the continued interest in these molecules. For example, a recent review highlighted the utility of heavy-element dithiocarbamato species as synthetic precursors for the generation of heavy-element sulfide nanomaterials [66] and this has been an important motivation for many studies on $Hg(S_2CNRR')_2$ molecules, some of which prove useful for the generation of the different polymorphs of HgS. A listing of the known structures of $Hg(S_2CNRR')_2$ is given in Table 1; examples with a functionalized dithiocarbamato ligand, for example, where the organic substituent bears a pyridyl residue and where residue coordinates to mercury, are not included in Table 1 as these have been reviewed in some detail recently [9]. The data in Table 1 are arranged in the following fashion: molecules are arranged in order of the structural motif, that is, binuclear, mononuclear (quasi-dimeric, tetrahedral, and square planar), one dimensional (zigzag, linear, and twisted topologies), and two dimensional. Within each category, molecules with identical R substituents, that is, $Hg(S_2CNR_2)_2$, are listed before dissymmetric molecules, $Hg(S_2CNRR')_2$, with molecules featuring cyclic substituents listed next. The final category lists multicomponent crystals, following the established order in terms of the substituents on the dithiocarbamato ligand.

Table 1. Summary of structural motifs adopted in X-ray crystal structures of $Hg(S_2CNR_2)_2$, $Hg(S_2CNRR')_2$, and their solvates.

First Substituent	Second Substituent	Recode	Ref.
Binuclear motif:			
R = Et	R = Et	HGETCB13	[41]
R = nPr	R = nPr	HUKCAU	[67]
R = iPr	R = iPr	ZAVYED	[68]
R = nBu	R = nBu	CAZRAW	[42]
R = CH_2(2-furyl)	R = CH_2(2-furyl)	ROVTED	[69]
R = Me	R′ = Ph	HAKKIP	[70]
R = Me	R′ = CH_2CH_2Ph	YABJIV	[71]
R = Me [a] R = Et	R′ = Ph R′= Ph	OROHEJ	[72]
R = Me [a] R = nBu	R′ = Ph R′ = Ph	HAGLOS	[73]
R = Et	R′ = Cy	CAZQUP	[42]
R = iPr	R′ = CH_2CH_2OH	OWOHUF	[35]
R = Et	R′ = Ph	YEDQEE	[74]
R = nBu	R′= CH_2(2-pyrrolyl)	ITEGUL	[75]
R = nBu	R′ = R1 [b]	XOHBAZ	[76]
R = CH_2CH_2OH	R′ = CH_2(Fc) [c]	EJAYOF	[77]
R = CH_2Ph	R′ = CH_2(2-furyl)	ROVVAB	[69]
R = CH_2CH_2Ph	R′ = CH_2(2-furyl)	TUMDOW	[78]
R = CH_2(2-furyl)	R′ = CH_2CH_2(2-thienyl)	TULJIV	[78]
R = CH_2(3-pyridyl)	R′ = CH_2(Fc) [c]	UTEKEL	[79]
NRR′ = $N(CH_2)_4$		DUWSIY	[80]
NRR′ = $N(CH_2)_5$		POGSUC	[81]
NRR′ = $N(CH_2)_6$		VOHKUZ	[82]
NRR′ = 4-methylpiperidine		KAFFIG	[83]
NRR′ = 4-benzylpiperidine		QAJNAU	[84]
NRR′ = 1,2,3,4-dihydroquinoline		SODNEG	[85]
Quasi-dimeric motif:			
R = Et [a] R =nBu	R = Ph R = Ph	YEQFEI	[86]
R = nPr	R = nPr	HUKCAU	[67]
R = iBu	R = iBu	CAZQID	[42]
R = CH_2Ph	R = CH_2Ph	ATADEE	[87]
R = iPr	R′ = Cy	CAZQOJ	[42]
R = nBu	R′= CH_2(2-pyrrolyl)	ITEGOF	[75]
R = CH_2Ph	R′ = CH_2(N-methyl-pyrrol-2-yl)	YOMYUW	[88]
R = CH_2Ph	R′ = CH_2(Fc) [c]	MUYXOU	[89]
NRR′ = 4-(3-phenylprop-2-en-1-yl)piperazine		LIFFEN	[90]

Table 1. *Cont.*

First Substituent	Second Substituent	Recode	Ref.
Tetrahedral motif:			
R = iPr	R = iPr	IPTCHG	[91,92]
R = Cy	R = Cy	ROPQIW	[43]
R = Et	R′= $CH_2C_6H_2(OMe)_3$-3,4,5	NIMWEO	[93]
R = CH_2(3-pyridyl)	R′ = CH_2(N-methyl-pyrrol-2-yl)	XOBCEY	[94]
R = CH_2(4-pyridyl)	R′ = CH_2(N-methyl-pyrrol-2-yl)	YOMYOQ	[88]
NRR′ = $N(CH_2)_4$		MUWDOX	[95]
Square-planar motif:			
R = $C_6H_3(iPr)_2$-2,6	R′ = $C(H)=NC_6H_3(iPr)_2$-2,6	VUWLUX	[96]
One dimensional: zigzag:			
R = CH_2CH_2Ph	R′ = CH_2(3-pyridyl)	FODROH	[97]
One dimensional: linear:			
R = Et	R = Et	HGETCB01	[98]
R = CH_2CH_2OH	R = CH_2CH_2OH	FOPWAJ	[99]
R = CH_2Ph	R′ = CH_2(3-pyridyl)	FODSAU	[97]
R = CH_2Ph	R′ = CH_2(4-pyridyl)	EBUTAY	[100]
NRR′ = $N(CH_2)_4$		POLNEM	[101]
One-dimensional: twisted:			
R = Me	R = Me	ROQNEQ	[102]
R = CH_2(3-pyridyl)	R′ = CH_2(3-pyridyl)	YOMYIK	[88]
R = $C_6H_3Me_2$-2,5	R′ = $C(H)=N(C_6H_3Me_2$-2,5)	VUWLOR	[96]
NRR′ = 1,2,3,4-dihydroquinoline		SODNIK	[85]
Two-dimensional:			
R = H	R = H	BAWWOL	[103]
Multicomponent crystals:			
R = Et [d]	R = Et	QIYTOI	[104]
R = Et [e]	R′ = Ph	AXIQEF	[105]
R = $C_6H_3Me_3$-2,4,6 [f]	R′ = $C(H)=NC_6H_3Cl_2$-2,5	VUWMAE	[96]
NRR′ = $N(CH_2CH_2)NPh_2$ [g]		QAJMUN	[84]
NRR′ = 1,2,3,4-dihydroquinoline [h]		SODNEG	[85]
NRR′ = 1,2,3,4-dihydroquinoline [i]		SODNIK	[85]
NRR′ = 1,2,3,4-dihydroquinoline [j]		SODNAC	[85]

[a]—The three entries highlighted in blue are mixed ligand species. [b]—The R′ group is: [c]—Fc is ferrocenyl, $(C_5H_4)Fe(C_5H_5)$. [d]—1:1 cocrystal with C_{60}. [e]—1:0.75 solvate with toluene. [f]—1:0.5 solvate with CH_2Cl_2. [g]—1:1 solvate with DMSO. [h]—1:1 solvate with pyridine. [i]—1:0.25 solvate with ethanol. [j]—1:1 cocrystal with 2,2′-bipyridine.

There are eight distinct structural motifs for molecules of the general formula $Hg(S_2CNRR')_2$ in their unsolvated crystals, with simplified images for these given in Figures 2–5. Of these motifs, four are zero dimensional. The most prominent motif among the 52 examples is a binuclear motif, found in 25 crystals, that is, nearly 50%. Here, one dithiocarbamato ligand is chelating, as is the second ligand, but this also simultaneously connects to the second Hg atom, Figure 2a. The second motif, Figure 2b, is closely related, but the intermolecular Hg···S separation is beyond the standard sum of the benchmark van der Waals radii (3.35 Å [45]). There are nine examples of this motif making this the second most popular motif. The remaining zero-dimensional motifs are mononuclear, there being no evidence of an intermolecular Hg···S contact. The difference between the latter motifs is in the coordination geometry, being based on a tetrahedron, Figure 2c, or a square planar geometry, Figure 2d. There are six examples of tetrahedral motifs and only a single example of the square planar motif.

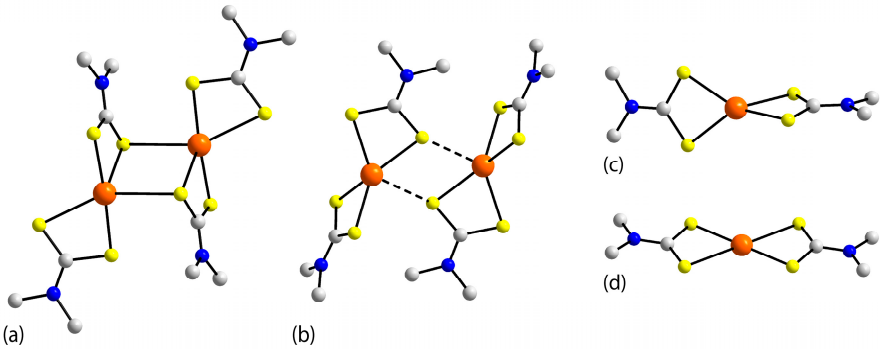

Figure 2. Simplified images for the four zero-dimensional structural motifs observed in the crystals of $Hg(S_2CNRR')_2$: (**a**) binuclear, (**b**) quasi dimeric, (**c**) tetrahedral, and (**d**) square planar. Color code: Hg, orange sphere; S, yellow; N, blue; C, gray; H, bright-green. For clarity, only the N-bound C atoms are shown.

Three different topologies of the chains are noted for the three one-dimensional motifs, that is, zigzag (one example), linear (five), and twisted (four). Representations of the chains are given in Figure 3a–c where side- and end-on views of the chains are illustrated, which clearly differentiate between the topologies.

There is a sole example of a two-dimensional structural motif, as represented in Figure 4. It is likely that weak N–H···S hydrogen bonding contributes to the stability of this motif in which all dithiocarbamato ligands are bidentate bridging.

As noted from Table 1, some molecules adopt more than one structural motif. A prime example is for the R = R = Et species which adopts both the binuclear motif [41] as well as the linear chain motif [98]. Another pair of motifs has been reported for the R = R = iPr compound, which can be a binuclear [68] or mononuclear tetrahedral [91,92]. These observations underscore the fascinating structural flexibility exhibited by these compounds in their crystals. While these multiple motifs are sometimes described as being polymorphs, a more correct terms might be a supramolecular isomerism [106,107] as the nature of the bonding between Hg and S is not necessarily the same.

For completeness, the motifs in seven multicomponent crystals are now summarized, Table 1. The R = R = Et species has been cocrystallized with fullarene with the retention of the binuclear motif [104]. Similarly, the binuclear motif for the R = Et and R'= Ph compound [74] is retained when the compound is crystallized with toluene [105]. There is no unsolvated precedent for the dissymmetric R = $C_6H_3Me_3$-2,4,6 and R' = C(H)=$NC_6H_3Cl_2$-2,5 compound which, as its CH_2Cl_2 solvate, adopts a twisted, one-dimensional coordination polymer [96]. Crystals of NRR' = $N(CH_2CH_2)NPh_2$, again, have not been isolated solvent-free, but when crystallized with DMSO, a mononuclear tetrahedral motif is seen [84]. A far more remarkable crystal chemistry is apparent for the compound with NRR' = 1,2,3,4-dihydroquinoline.

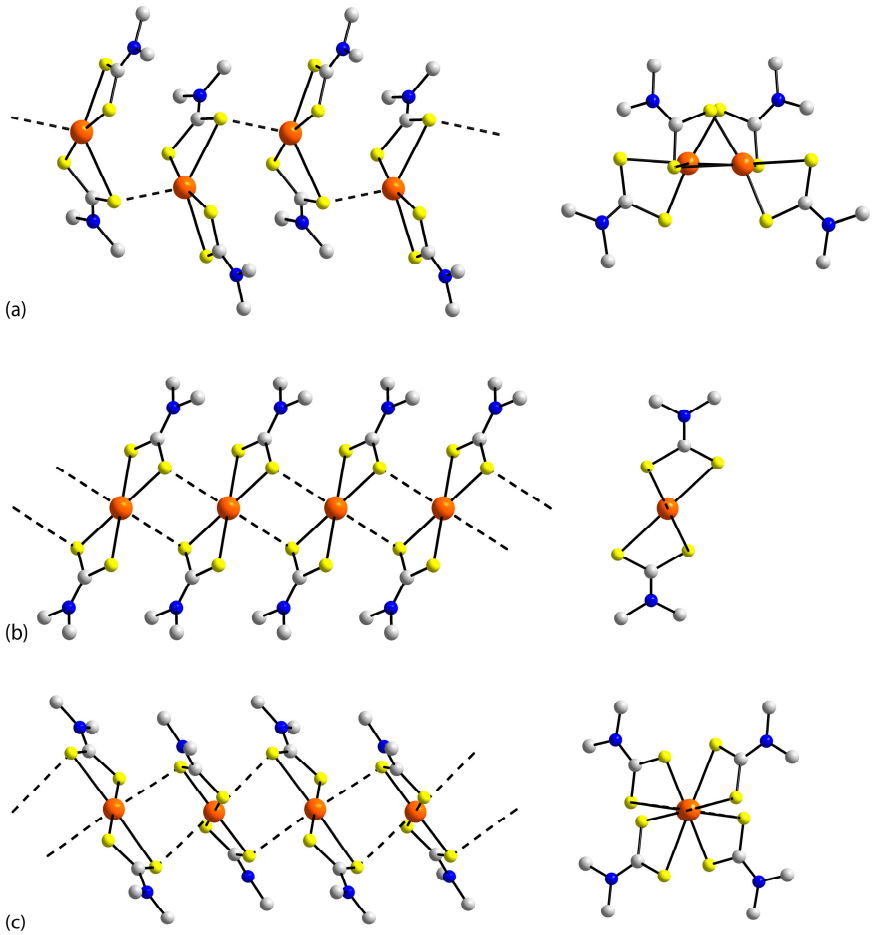

Figure 3. Simplified images for the three one-dimensional structural motifs observed in the crystals of $Hg(S_2CNRR')_2$: (**a**) zigzag chain, (**b**) linear chain, and (**c**) twisted chain.

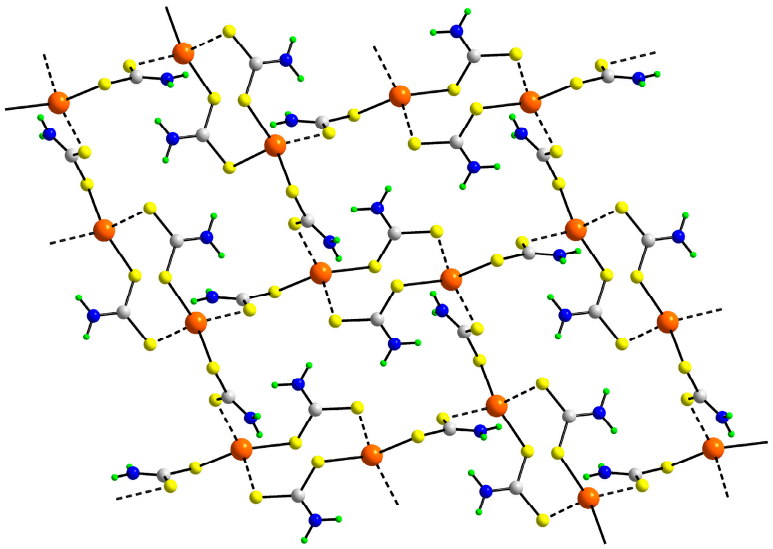

Figure 4. Simplified image for a two-dimensional array.

The solvent-free species with NRR′ = 1,2,3,4-dihydroquinoline is a twisted coordination polymer [85] and there are three other structures known, each with a cocrystallized solvent [85]. With 2,2′-bipyridine, the twisted coordination polymer, as for the unsolvated species, persists, but with EtOH, the binuclear motif is observed. When the solvent is

pyridine, a new structural motif is observed; the disordered pyridine molecule does not interact with Hg. As seen from Figure 5, a zero-dimensional trinuclear motif is seen in the pyridine solvate. The molecule is centrosymmetric and combines the elements of the binuclear motif, Figure 2a, and square planar motif, Figure 2d, with the former flanking the latter with long Hg···S connections [85].

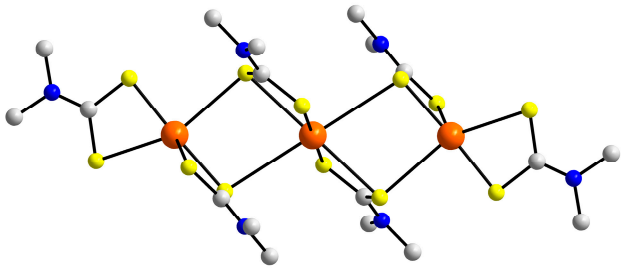

Figure 5. Simplified images for an additional zero-dimensional structural motif.

While the elucidation of the structures found in the solid state for $Hg(S_2CNRR')_2$ molecules in their crystals is important and of interest, far more challenging is to rationalize the appearance of the different motifs. In order to do this, careful and comparative experiments are required in contrast to the myriad of crystallization conditions employed for the generation of $Hg(S_2CNRR')_2$ crystals, such as the choice of solvent, the duration of crystallization, concentration, temperature, etc. Recently, such trials were performed for closely related $Cd[S_2CN(iPr)CH_2CH_2OH]_2$ compound [108]. For example, in ethanol solutions, needles of the coordination polymer $\{Cd[S_2CN(iPr)CH_2CH_2OH]_2{\cdot}EHOH\}_\infty$ formed within three hours of recrystallization which, after another hour, had converted quantitatively to the usually observed binuclear motif as prisms and as the di-EtOH solvate. It was concluded that the least soluble coordination polymer initially crystallized which promptly reverted to the thermodynamic (binuclear) form [108]. In the present study, the focus is upon the relationship between the prominent binuclear form and mononuclear species. Specifically, insight is sought regarding the role of the steric bulk of dithiocarbamato-bound alkyl groups upon the adoption of the mononuclear motifs as opposed to the binuclear motif and any role spodium bonding has upon the supramolecular aggregation. The $Hg(S_2CNRR')_2$ molecules chosen for study, that is, with R = R′= ethyl (**1**), isobutyl (**2**), and cyclohexyl (**3**), were found in solvent-free crystals and had symmetric R groups and featured alkyl substituents in order to negate any influence of interactions involving π systems.

3.2. Experimental Structures

Two distinct coordination modes are noted for the dithiocarbamato anions in the crystal of **1**. As noted in Figure 6a, one ligand is bound to one Hg center and simultaneously bridges a second Hg atom related to the first over an inversion center. Key bond lengths and angles for **1**–**3** are listed in Table 2. These data indicate the Hg–S1, and S2 ^{i} bridging bond lengths in **1** differ by approximately 0.10 Å, indicating the bridge is close to symmetrical. With the difference in the Hg–S3, the S4 bond lengths for the second independent dithiocarbamato ligand being 0.12 Å, this ligand coordinates in the chelating mode. The result of the bridging mode of coordination is the formation of an eight-membered $\{–HgSCS\}_2$ core which has the shape of an extended chair whereby the two pairs of C and S1 atoms lie above the plane of the remaining atoms. Also noted from Figure 6a is the presence of transannular Hg···S2 interactions which are considered long at 3.1266(9) Å, but nevertheless, are shorter than the sum of the van der Waals radii of Hg (1.55 Å) and S (1.80 Å), that is, 3.35 Å [45].

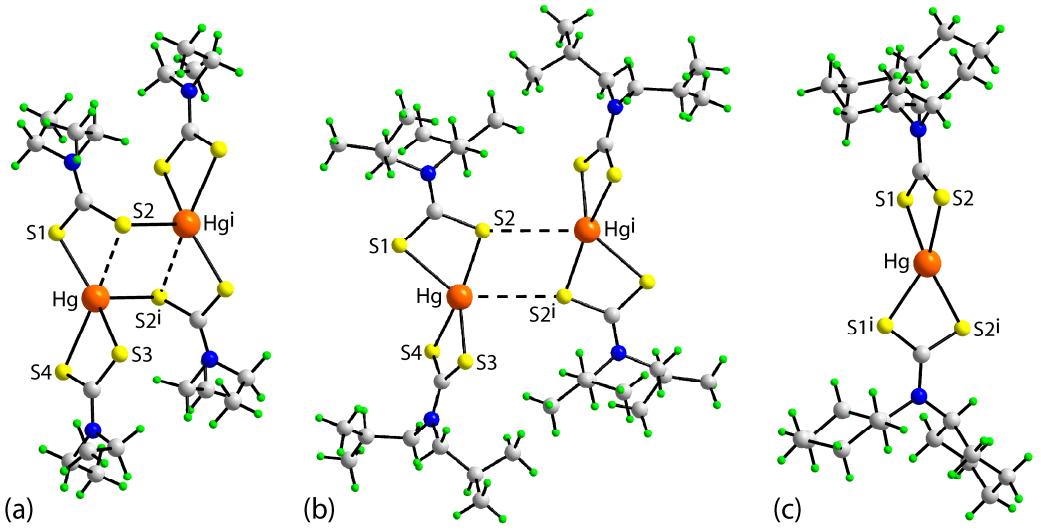

Figure 6. Supramolecular aggregation via Hg–S/Hg···S interactions in the crystals of $Hg(S_2CNR_2)_2$: (**a**) R = ethyl (**1**), (**b**) R = isobutyl (**2**), and (**c**) the monomeric molecule for R = cyclohexyl (**3**). Symmetry operations i in (**a**) and (**b**) are given in Table 2.

Table 2. Selected geometric parameters (Å, °) about the Hg centers in the crystals of $Hg(S_2CNR_2)_2$: R = ethyl (**1**), R = isobutyl (**2**), and R = cyclohexyl (**3**).

Parameter	1	2	3 [a]
Hg–S1	2.4216(11)	2.710(3)	2.527(3)
Hg–S2	3.1266(9)	2.438(2)	2.536(4)
Hg–S3	2.5183(10)	2.417(3)	2.527(3)
Hg–S4	2.6408(10)	2.714(3)	2.536(4)
S2–Hg [i]	2.6725(10)	3.727(4)	-
S1–Hg–S2	63.87(3)	70.43(9)	71.69(10)
S1–Hg–S3	144.88(3)	126.57(9)	129.87(16)
S1–Hg–S4	122.28(3)	105.96(9)	126.07(9)
S2–Hg–S3	92.98(3)	153.92(8)	126.07(9)
S2–Hg–S4	157.70(3)	127.92(9)	142.18(18)
S3–Hg–S4	70.40(3)	70.58(9)	71.69(10)
S1–Hg–S2 [i]	107.96(3)	131.64(7)	-
S2–Hg–S2 [i]	100.81(3)	76.04(6)	-
S3–Hg–S2 [i]	101.89(3)	78.20(6)	-
S4–Hg–S2 [i]	97.22(3)	122.14(7)	-
Hg–S2 [i]–Hg [i]	79.19(3)	103.96(6)	-
Symmetry			
operation [i]	−x, −y, 1 − z	$\frac{1}{2}$ − x, $\frac{1}{2}$ − y, −z	-

[a]—The Hg atom in **3** is located on a two-fold axis of symmetry, so S3 = S1 [ii] and S4 = S2 [ii] (symmetry operation ii: x − y, −y, 2/3 − z).

In **2**, Figure 6b, the two independent dithiocarbamato ligands coordinate in a similar fashion with the differences in the pairs of Hg–S1, S2, and Hg–S3, with the S4 bond lengths being 0.27 and 0.29 Å, respectively. Centrosymmetrically related molecules approach each other to potentially form Hg···S interactions, but the separation between the atoms is rather long at 2.727(4) Å. The putative supramolecular synthon is a centrosymmetric,

four-membered $\{\cdots HgS\}_2$ synthon, often observed in the supramolecular chemistry of crystals containing both Hg and S [38,39]. In **3**, Figure 6c, the Hg atom is located on a two-fold axis of symmetry. The difference in the Hg–S1, S2 bond lengths is only 0.01 Å. No evidence for Hg···S interactions is present in the crystal of **3**.

Figure 7 highlights the versatility in the coordination modes adopted by the dithiocarbamato ligands in **1**–**3**. The dimer in **1** exhibits bonding modes based on (a) and (b), **2** exhibits coordination modes intermediate between (a) and (c), whereas in **3**, the coordination mode is that shown in Figure 7a. As a generalization, the bridging modes of coordination for dithiocarbamato anions are more likely for Group 12 and p block elements than for transition metals [1–10].

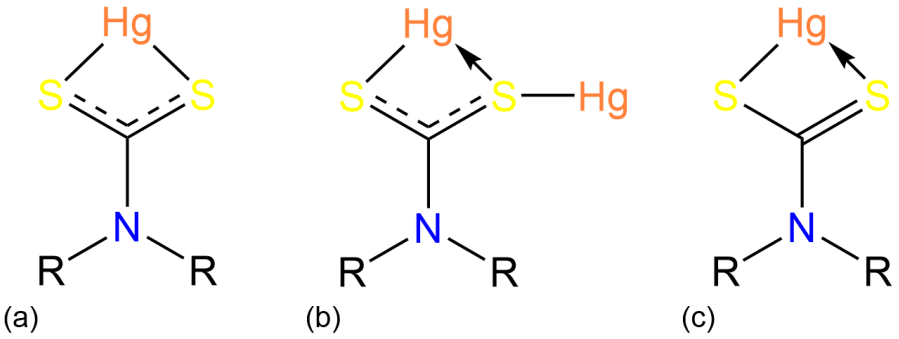

Figure 7. Variable coordination modes of the dialkyldithiocarbamato anion towards mercury(II): (**a**) symmetric chelating with similar Hg–S bond lengths, (**b**) bidentate bridging with approximately similar Hg–S bond lengths, and (**c**) asymmetric chelating with dissimilar Hg–S bond lengths.

To a first approximation, the Hg atom in **1** is pentacoordinated within a S_5-donor set owing to the transannular Hg···S2 interaction. A useful geometric parameter for assessing five coordinated centers is the computed τ_5 value, which for an ideal square-pyramidal geometry is 0.0 and for an ideal trigonal-bipyramid is 1.0 [109]. For **1**, the value of τ_5 is 0.21, clearly consistent with a distorted geometry approaching a square pyramid. In this description, the bridging S2 ^{i} atom occupies the apical position. The distortions arise, in part, due to the acute chelate angles formed by the dithiocarbamato ligands and the close approach of weakly bound S2 atoms, Table 2. In each of **2** and **3**, the Hg atom is tetracoordinated within a S_4 donor set. The analogous geometric parameter for four coordinated species, τ_4, adopts values of 0.00 for an ideal square planar geometry, 1.00, for an ideal tetrahedron and, between these extremes, τ_4 = 0.85, for a trigonal pyramidal geometry [110]. In **2** and **3**, τ_4 has values of 0.55 and 0.62, respectively, again indicating distorted geometries which are closer to trigonal-pyramidal. There are also conformational differences between **1**, where the dihedral angle formed between the two chelate rings bound to the same Hg atom is 30.46(3)°, compared with the significantly greater angles in **2** [82.29(7)°] and **3** [79.8(5)°], indicating near to the perpendicular arrangements between the chelate rings in the latter.

Space-filling diagrams [47] for the dimeric aggregates in **1** and **2** and for the monomer in **3** are illustrated in Figure 8a–c. Qualitatively, increasing the steric bulk of the nitrogen-bound R groups from ethyl in **1** to isobutyl in **2** precludes the closer approach of the molecules in the latter. From the image in Figure 8c, the cyclohexyl groups are too large to prevent any semblance of an intermolecular Hg–S/Hg···S interaction.

Table 3 lists some key parameters describing the molecular volumes of **1**–**3**, being calculated with MoloVol [46]. From the data included in Table 3, it is clear there is a systematic variation in the calculated volumes for the individual molecules, even allowing for void space which decreases in the order **1** [10.1%] > **2** [6.6%] > **3** [2.2%], consistent with more efficient close packing as the importance of the intermolecular Hg–S/Hg···S interactions decreases. Similar conclusions are evident from the analysis of the calculated Hirshfeld surfaces for **1**–**3**.

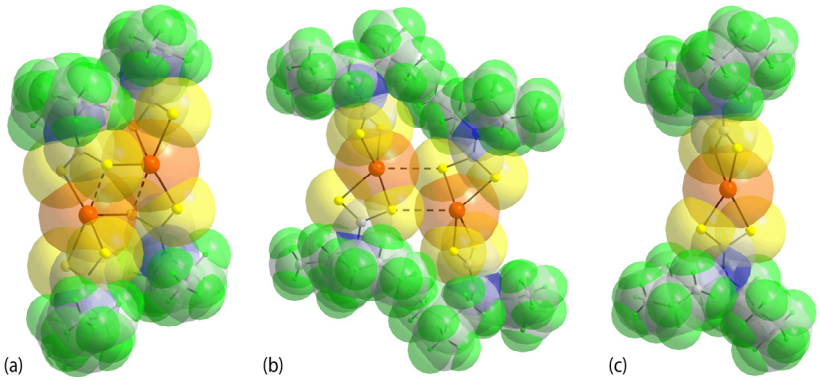

Figure 8. Space-filling images for the dimeric aggregates in the crystals of $Hg(S_2CNR_2)_2$ for (**a**) R = ethyl (**1**) and (**b**) R = isobutyl (**2**), and (**c**) for the monomeric molecule when R = cyclohexyl (**3**).

Table 3. Calculated volumes ($Å^3$) for the molecules in the crystals of $Hg(S_2CNR_2)_2$: (a) R = ethyl (**1**), (b) R = isobutyl (**2**), and (c) R = cyclohexyl (**3**).

Parameter	1	2	3 [a]
van der Waals volume [a]	588.2/294.1	431.3	814.8
Probe-excluded void volume [a]	59.4/29.7	28.5	17.9
Molecular volume [a]	647.6/323.8	459.7	832.6

[a]—The second values for **1** are for the monomer.

Figure 9 plots the four most prominent calculated surface contacts in the crystals of **1**–**3**, that is, H···H, H···S/S···H, H···C/C···H, and H···Hg/Hg···S; hydrogen is involved in 99.9, 98.2, and 100.0% of all contacts in the crystals of **1**–**3**, respectively. For **1**, the calculations were performed on the dimeric aggregate. The H···H contacts are clearly the most dominant across the series and increase in the order **1** [55.0%] < **2** [66.9%] < **3** [69.1%]. The next most dominant contacts, H···S/S···H, follow the inverse trend, that is, **1** [37.2%] > **2** [25.9%] > **3** [23.7%]. There is a large fall in the percentage contributions to the next most important H···C/C···H and H···Hg/Hg···S surface contacts which do not manifest obvious trends. The remaining surface contacts contribute less than 1% to the respective Hirshfeld surfaces with H···N/N···H more important in **1** [0.7%] compared with 0.1% in the crystals of **2** and **3**. Surface contacts due to S···S are more significant in **2** [0.7%] as opposed to **1** [0.1%] and **3** [0.0%], and the same is true for Hg···H/H···Hg [0.6%] in contrast to the 0.0% contributions in **1** and **3**.

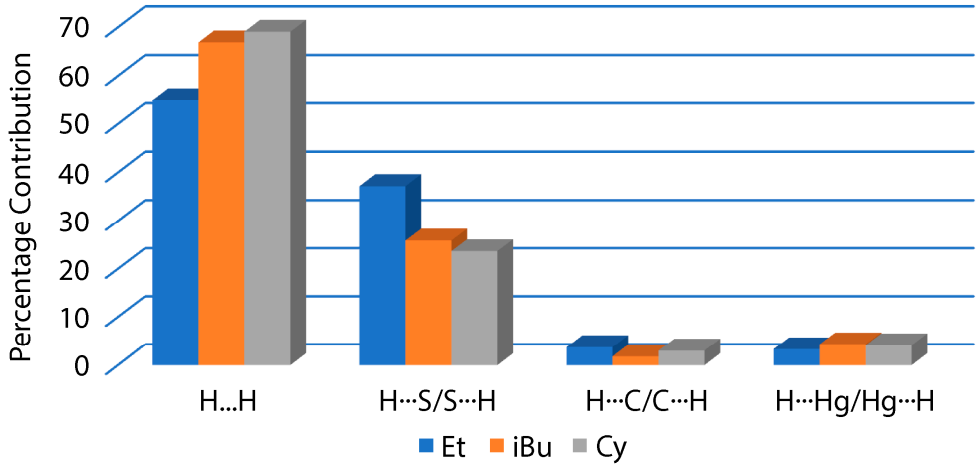

Figure 9. A bar graph contrasting the percentage contributions of the four major contacts to the calculated Hirshfeld surfaces of $Hg(S_2CNR_2)_2$ for R = ethyl (**1**), R = isobutyl (**2**), and R = cyclohexyl (**3**).

The foregoing affirms the structural diversity of $Hg(S_2CNR_2)_2$ molecules, at least for the zero-dimensional R = ethyl (**1**), R = isobutyl (**2**), and R = cyclohexyl (**3**) series. A consequence of these variations is a distinct pattern of Hg···S secondary bonding interactions, namely intramolecular, intermolecular, and none for **1**–**3**, respectively. In order to ascertain the nature of these Hg···S interactions and the influence of the adopted molecular structures on their formation, molecules **1**–**3** were subjected to density-functional theory (DFT) calculations.

3.3. DFT Calculations

A thorough DFT study has been conducted to better understand and describe the presence of Hg···S interactions, shown below to be spodium bonds (SpBs) in crystals of $Hg(S_2CNR_2)_2$ for R = ethyl (**1**) and R = isobutyl (**2**), that is, intra- and intermolecular SpBs, respectively, and the absence of SpBs when R = cyclohexyl (**3**). Firstly, to assess the presence and accessibility of the π-hole on the Hg atoms in **1**–**3**, their MEP surfaces were computed.

For **1**, the optimization of the isolated $Hg(S_2CNEt_2)_2$ fragment revealed two distinct minima. The more stable configuration has a pseudo-tetrahedral coordination. The less stable configuration, higher in energy by +3.2 kcal/mol, features a linear S–Hg–S coordination with two auxiliary Hg···S contacts and a coplanar arrangement of the four S atoms, Figure 10a. Notably, the MEP surface plots differ between the two isomers: only the coplanar form has a positive potential region at the Hg atom (+6.9 kcal/mol), while the pseudo tetrahedral form shows a slightly negative MEP at the Hg position. However, the MEP maxima and minima are comparable for both configurations. These findings on the isolated geometry-optimized $Hg(S_2CNEt_2)_2$ fragments, having either square planar or tetrahedral geometries, imply that the existence of SpBs is closely tied to the coordination sphere/geometry about the Hg atom.

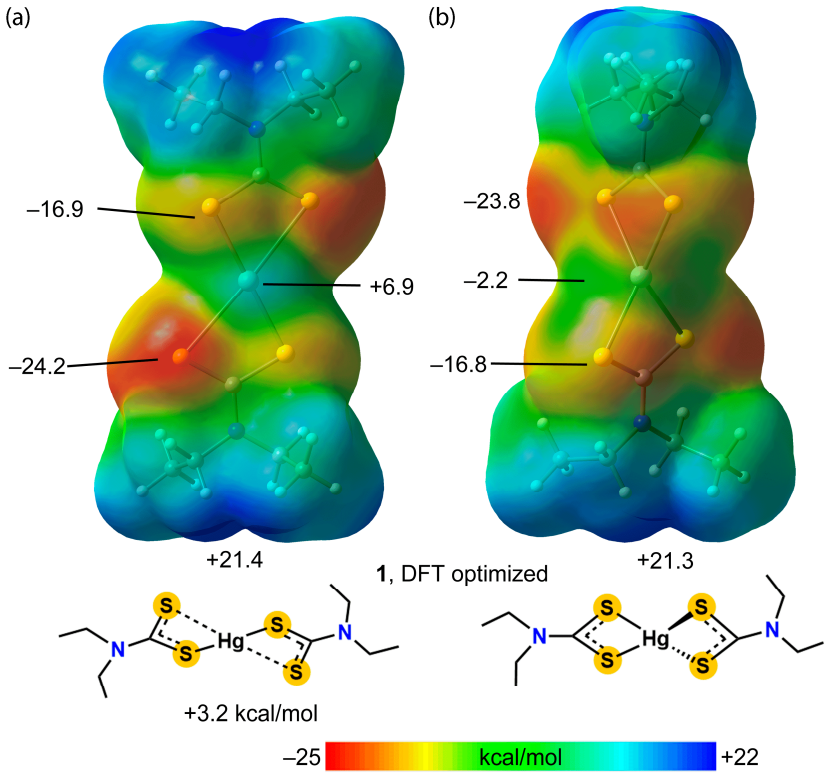

Figure 10. MEP surface plots for the optimized $Hg(S_2CNEt_2)_2$ fragment of **1**: (**a**) planar and (**b**) pseudo-tetrahedral configurations. The MEP values at selected points are given in kcal/mol.

Figure 11 illustrates the MEP surfaces for the isolated molecules in **2** and **3**, based on their X-ray-determined geometries. This helps clarify the presence or absence of SpBs in

their respective solid-state structures. Intriguingly, **2** (R = isobutyl) exhibits a flat pseudo-trigonal geometry with three primary Hg–S coordination bonds and an additional ancillary Hg···S bond. This compound reveals a positive potential region at the Hg atom (+4.5 kcal/mol), which is somewhat less pronounced than that in compound **1** (with a linear coordination, as seen in Figure 11a). For **3** (R = cyclohexyl), its MEP surface plot indicates a negative potential at the Hg atom, likely attributed to its pseudo-tetrahedral coordination. Therefore, the absence of SpB contacts in **3** can be attributed to its pseudo-tetrahedral coordination and the associated lack of a positive MEP.

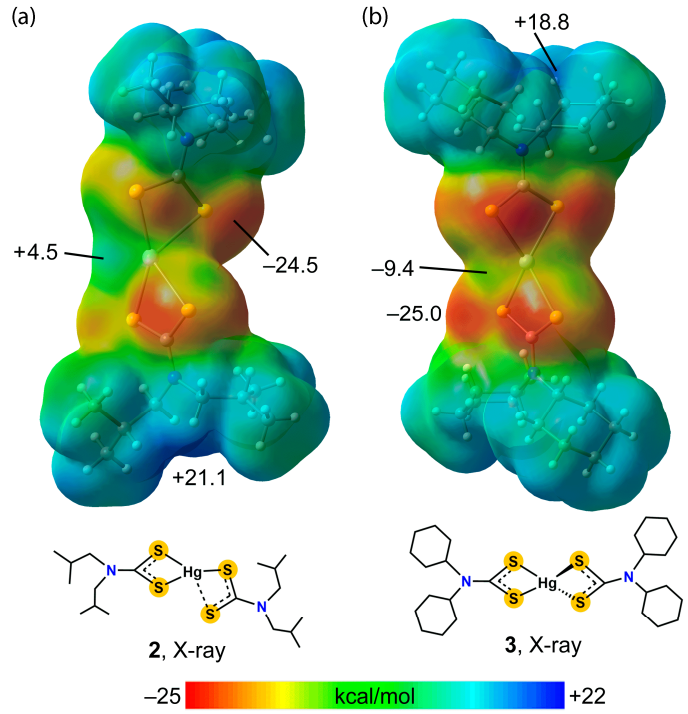

Figure 11. MEP surface plots calculated for the X-ray geometries of (**a**) **2** and (**b**) **3**. The MEP values at selected points are given in kcal/mol.

The SpBs in **1** (intramolecular) and **2** (intermolecular) have been thoroughly examined using a combination of QTAIM and NCIplot analyses. While the use of QTAIM for the analysis of noncovalent interactions is sometimes debated [111–114], our experience shows this is a useful complementary tool in the study of these inherently weak interactions, including for mercury-containing compounds [19,39], as combined QTAIM and NCIplot methods effectively visualize noncovalent interactions in real space. For **1**, the intramolecular SpBs feature a bond critical point (BCP, shown as a red sphere) and a bond path linking the Hg and S atoms, Figure 12a. The disk-shaped reduced density gradient (RDG) isosurface aligns with the location of the BCP. The light-blue color along with the density value at the BCP (0.0226 a.u.) highlight the moderately strong nature of these SpBs. For **2**, the supramolecular dimer was studied (Figure 12b). The QTAIM/NCIplot findings confirm the presence of the Hg···S SpBs, marked by their respective BCPs, bond paths, and green RDG isosurfaces. The color of the RDG isosurfaces indicates that these intermolecular SpBs are weaker than the intramolecular SpBs in **1**, consistent with the longer separations and a smaller BCP density (0.0065 a.u.). Further, the analysis reveals additional CH···S contacts aiding dimer formation. The dimerization energy stands at –11.7 kcal/mol, incorporating both the SpBs and CH···S contacts. As a first approximation [115], to isolate the contribution of SpBs, a modified dimer was analyzed where $–NR_2$ (R = cyclohexyl) in **3** was substituted with $–NH_2$ groups. This change eliminates the CH···S contacts and other van der Waals CH···HC interactions, lowering the interaction energy to −4.9 kcal/mol. This suggests each SpB contributes about −2.5 kcal/mol, corroborated

by the color of the RDG isosurface, the small density at the BCP, and the minimal MEP value at the Hg atom, Figure 12a. This observation is in keeping with the notion that SpBs provide energies of stabilization [19,39] comparable to other supramolecular association modes like hydrogen bonding [116]. Indeed, this energy is rather remarkable given the long separation between the Hg and S atoms forming the Hg···S SpB, further supporting the idea that significant structure-directing interactions can exist at distances greater than the sum of the conventional van der Waals radii [117–120].

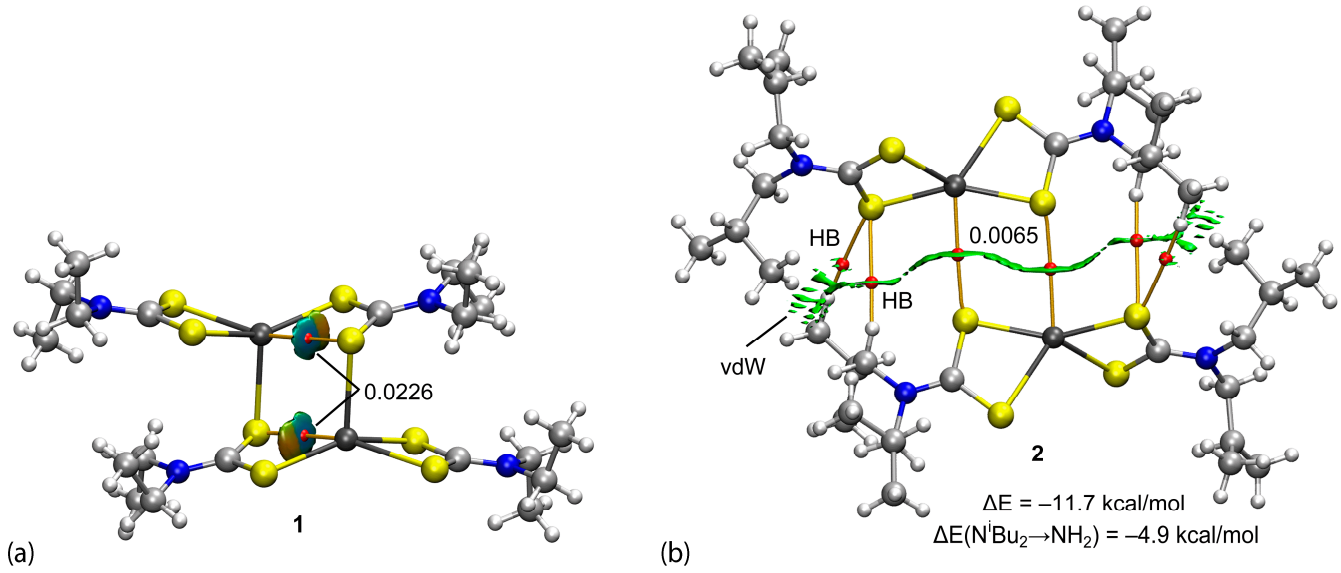

Figure 12. QTAIM (BCPs in red and bond paths as orange lines) and NCIplot (RDG = 0.5, ρ cutoff = 0.04 a.u., color scale –0.035 a.u. $\leq$ (signλ_2)ρ $\leq$ 0.035 a.u.) for (**a**) **1** and (**b**) the weakly associated dimer in **2**. The dimerization energies for (**b**) are also indicated. The values of ρ at the BCPs are given in a.u. "HB" refers to the CH···S contact and "vd W" is van der Waals.

The interactions in **2** were further evaluated using the NBO method, an approach well suited for probing donor/acceptor interactions and analyzing charge transfer effects. Notably, the analysis revealed an electron donation from a lone pair orbital at the S atom of one monomer to the antibonding Hg–S orbital of its counterpart, and vice versa (with only one set depicted in Figure 13). This results in a total stabilization energy of $E^{(2)}$ = 1.8 kcal/mol, equating to 0.9 kcal/mol for each LP(S) → σ*(Hg–S) donor/acceptor interaction.

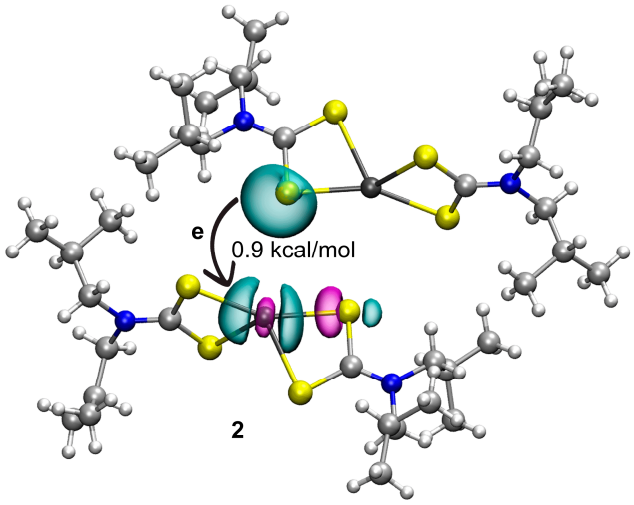

Figure 13. NBOs involved in the LP(S) → σ*(Hg–S) donor/acceptor interaction in **2**. The second-order perturbation energy is indicated.

To probe the physical nature of intermolecular interactions within the self-assembled dimer of **2**, an EDA was conducted. Figure 14 presents the results of this analysis through a bar plot. The data reveal that the correlation (E_{cor}, lilac bar) and dispersion (E_{disp}, green bar) contributions are more significant than the electrostatic (Eel, blue bar) and orbital (E_{orb}, grey bar) components. This observation accounts for the substantial dimerization energy recorded for the dimer of **2** (E_{tot} = −11.7 kcal/mol, pink bar), despite the minimal MEP value at Hg and the minor LP(S) → σ*(Hg–S) charge transfer identified from the MEP surface and NBO analyses. Notably, dispersion is the primary contributor, succeeded by the electron correlation. This is associated with the participation of a heavy metal (increasing E_{cor}) and the CH···HC interactions (increasing E_{disp}) between the alkyl chains, further supported by the NCIplot analysis (Figure 12b).

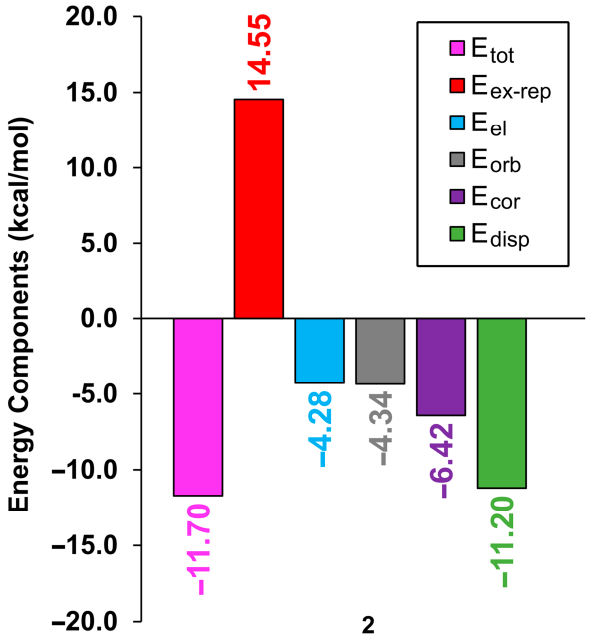

Figure 14. Total (E_{tot}), exchange repulsion (E_{ex-rep}), electrostatic (E_{el}), orbital (E_{orb}), correlation (E_{cor}), and dispersion (E_{disp}) for the dimer in the crystal of **2**. Energies are given in kcal/mol.

4. Conclusions

Steric effects associated with the dithiocarbamato-bound R substituents are crucial in determining the mode of coordination of the dithiocarbamato anions in $Hg(S_2CNR_2)_2$ crystals: the small ethyl substituents in **1** allow for a bridging mode of coordination, leading to dimer formation, but this is precluded by the larger substituents in **2** (isobutyl) and **3** (cyclohexyl). Using DFT analyses, the varying presence and nature of SpBs across compounds **1** to **3** was discerned, highlighting the significance of the coordination geometry and molecular electrostatic potential. The QTAIM and NCI plot analyses provided a clear depiction of noncovalent interactions, evidencing stronger SpBs in **1** (intramolecular) than **2** (intermolecular). In **2**, energetic assessments indicate a moderate SpB interaction strength, approximately −2.5 kcal/mol, despite the long separation between the interacting centers. Moreover, the NBO analysis of **2** highlights the LP(S) → σ*(Hg–S) charge transfer phenomenon. Finally, the study evidences the dominant dispersion forces followed by an electron correlation in the supramolecular dimer of **2**. This knowledge is expected to interest scientists across supramolecular chemistry, crystal engineering, coordination, and theoretical chemistry domains.

Supplementary Materials: The following supporting information can be downloaded at: https://www.mdpi.com/article/10.3390/inorganics11120468/s1, Table S1: QTAIM parameters (a.u.) for the

bond critical points that characterize the spodium bonds; Table S2: Cartesian coordinates for the geometry optimized monomeric molecules of **1**.

Author Contributions: Conceptualization, E.R.T.T.; formal analysis, R.M.G., E.R.T.T. and A.F.; investigation, R.M.G., E.R.T.T. and A.F.; writing—original draft preparation, R.M.G., E.R.T.T. and A.F.; writing—review and editing, R.M.G., E.R.T.T. and A.F.; visualization, R.M.G., E.R.T.T. and A.F.; funding acquisition, A.F. All authors have read and agreed to the published version of the manuscript.

Funding: This research was funded by MICIU/AEI of Spain, grant number PID2020-115637GB-I00 FEDER funds.

Data Availability Statement: The data presented in this study are available on request from the authors.

Acknowledgments: The authors thank CTI (UIB) for computational facilities.

Conflicts of Interest: The authors declare no conflict of interest.

References

1. Coucouvanis, D. The chemistry of the dithioacid and 1,1-dithiolate complexes. *Prog. Inorg. Chem.* **1970**, *11*, 234–371. [CrossRef]
2. Eisenberg, R. Structural systematics of 1,1- and 1,2-dithiolato chelates. *Prog. Inorg. Chem.* **1970**, *12*, 295–369. [CrossRef]
3. Coucouvanis, D. The chemistry of the dithioacid and 1,1-dithiolate complexes, 1968–1977. *Prog. Inorg. Chem.* **1979**, *26*, 301–469. [CrossRef]
4. Hogarth, G. Transition metal dithiocarbamates: 1978–2003. *Prog. Inorg. Chem.* **2005**, *53*, 71–561. [CrossRef]
5. Heard, P.J. Main group dithiocarbamate complexes. *Prog. Inorg. Chem.* **2005**, *53*, 1–69. [CrossRef]
6. Haiduc, I. 1,1-Dithiolato ligands and related selenium and tellurium compounds. In *Handbook of Chalcogen Chemistry*; Devillanova, F.A., Ed.; Royal Society of Chemistry: Cambridge, UK, 2007; pp. 593–643. ISBN 978-0-85404-366-8.
7. Tiekink, E.R.T. Molecular architecture and supramolecular association in the zinc-triad 1,1-dithiolates. Steric control as a design element in crystal engineering? *CrystEngComm* **2003**, *5*, 101–113. [CrossRef]
8. Tiekink, E.R.T. Exploring the topological landscape exhibited by binary zinc-triad 1,1-dithiolates. *Crystals* **2018**, *8*, 292. [CrossRef]
9. Tiekink, E.R.T. On the coordination role of pyridyl-nitrogen in the structural chemistry of pyridyl-substituted dithiocarbamate ligands. *Crystals* **2021**, *11*, 286. [CrossRef]
10. Lee, S.M.; Tiekink, E.R.T. A structural survey of poly-functional dithiocarbamate ligands and the aggregation patterns they sustain. *Inorganics* **2021**, *9*, 7. [CrossRef]
11. Mulliken, R.S. Structures of complexes formed by halogen molecules with aromatic and with oxygenated solvents. *J. Am. Chem. Soc.* **1950**, *72*, 600–608. [CrossRef]
12. Bent, H.A. Structural chemistry of donor-acceptor interactions. *Chem. Rev.* **1968**, *68*, 587–648. [CrossRef]
13. Hassel, O. Structural Aspects of interatomic charge-transfer bonding. *Science* **1970**, *170*, 497–502. [CrossRef] [PubMed]
14. Alcock, N.W. Secondary bonding to nonmetallic elements. *Adv. Inorg. Chem. Radiochem.* **1972**, *15*, 1–58. [CrossRef]
15. Legon, A.C. Tetrel, pnictogen and chalcogen bonds identified in the gas phase before they had names: A systematic look at non-covalent interactions. *Phys. Chem. Chem. Phys.* **2017**, *19*, 14884–14896. [CrossRef] [PubMed]
16. Edwards, A.J.; Mackenzie, C.F.; Spackman, P.R.; Jayatilaka, D.; Spackman, M.A. Intermolecular interactions in molecular crystals: What's in a name? *Faraday Discuss.* **2017**, *203*, 93–112. [CrossRef]
17. Scheiner, S.; Michalczyk, M.; Zierkiewicz, W. Coordination of anions by noncovalently bonded σ-hole ligands. *Coord. Chem. Rev.* **2020**, *405*, 213136. [CrossRef]
18. Brammer, L.; Peuronen, A.; Roseveare, T.M. Halogen bonds, chalcogen bonds, pnictogen bonds, tetrel bonds and other σ-hole interactions: A snapshot of current progress, Acta Crystallogr. *Sect. C Struct. Chem.* **2023**, *79*, 204–216. [CrossRef] [PubMed]
19. Bauzá, A.; Alkorta, I.; Elguero, J.; Mooibroek, T.J.; Frontera, A. Spodium bonds: Noncovalent interactions involving Group 12 elements. *Angew. Chem. Int. Ed.* **2020**, *59*, 17482–17487. [CrossRef] [PubMed]
20. Ciancaleoni, G.; Rocchigiani, L. Assessing the orbital contribution in the "spodium bond" by natural orbital for chemical valence−charge displacement analysis. *Inorg. Chem.* **2021**, *60*, 4683–4692. [CrossRef]
21. Liu, N.; Xie, X.; Li, Q. Chalcogen bond involving zinc(II)/cadmium(II) carbonate and its enhancement by spodium bond. *Molecules* **2021**, *26*, 6443. [CrossRef]
22. Wysokiński, R.; Zierkiewicz, W.; Michalczyk, M.; Scheiner, S. Anion$\cdots$anion $(MX^{3-})_2$ dimers (M = Zn, Cd, Hg; X = Cl, Br, I) in different environments. *Phys. Chem. Chem. Phys.* **2021**, *23*, 13853–13861. [CrossRef]
23. Singh, A.; Kociok-Köhn, G.; Dutta, A.; Kumar, A.; Muddassir, M. Diaminopyridine Hg(II)-based 1D supramolecular polymer: Crystallographic and computational insights into spodium bonding. *J. Solid State Chem.* **2022**, *315*, 123517. [CrossRef]
24. Kumar, P.; Banerjee, S.; Radha, A.; Firdoos, T.; Sahoo, S.C.; Pandey, S.K. Role of non-covalent interactions in the supramolecular architectures of mercury(II) diphenyldithiophosphates: An experimental and theoretical investigation. *New J. Chem.* **2021**, *45*, 2249–2263. [CrossRef]
25. Liu, N.; Li, Q.; Scheiner, S. Spodium and tetrel bonds involving Zn(II)/Cd(II) and their interplay. *Chem. Phys.* **2022**, *556*, 111470. [CrossRef]

26. Gao, M.; Zhao, Q.; Yu, H.; Fu, M.; Li, Q. Insight into spodium–π bonding characteristics of the $MX_2 \cdots \pi$ (M = Zn, Cd and Hg; X = Cl, Br and I) complexes—A theoretical study. *Molecules* **2022**, *27*, 2885. [CrossRef] [PubMed]
27. Rozhkov, A.V.; Katlenok, E.A.; Zhmykhova, M.V.; Kuznetsov, M.L.; Khrustalev, V.N.; Tugashov, K.I.; Bokach, N.A.; Kukushkin, V.Y. Spodium bonding to anticrown-Hg_3 boosts phosphorescence of cyclometalated-Pt^{II} complexes. *Inorg. Chem. Front.* **2023**, *10*, 493–510. [CrossRef]
28. Wu, Q.; McDowell, S.A.C.; Li, Q. Single-electron spodium bonds: Substituent effects. *Appl. Organomet. Chem.* **2023**, *37*, e7052. [CrossRef]
29. Clark, T.; Hennemann, M.; Murray, J.S.; Politzer, P. Halogen bonding: The sigma-hole. *J. Mol. Model.* **2007**, *13*, 291–296. [CrossRef]
30. Murray, J.S.; Lane, P.; Clark, T.; Politzer, P.J. σ-hole bonding: Molecules containing group VI atoms. *Mol. Model.* **2007**, *13*, 1033–1038. [CrossRef]
31. Kolář, M.H.; Hobza, P. Computer modeling of halogen bonds and other σ-hole interactions. *Chem. Rev.* **2016**, *116*, 5155–5187. [CrossRef]
32. Politzer, P.; Murray, J.S. σ-Hole interactions: Perspectives and misconceptions. *Crystals* **2017**, *7*, 212. [CrossRef]
33. Politzer, P.; Murray, J.S.; Clark, T.; Resnati, G. The σ-hole revisited. *Phys. Chem. Chem. Phys.* **2017**, *19*, 32166–32178. [CrossRef]
34. Murray, J.S.; Politzer, P. Interaction and polarization energy relationships in σ-hole and π-hole bonding. *Crystals* **2020**, *10*, 76. [CrossRef]
35. Jotani, M.M.; Tan, Y.S.; Tiekink, E.R.T. Bis[bis(N-2-hydroxyethyl,N-isopropyldithiocarbamato)mercury(II)]2: Crystal structure and Hirshfeld surface analysis. *Z. Kristallogr.—Cryst. Mater.* **2016**, *231*, 403–413. [CrossRef]
36. Winter, G. Inorganic xanthates. *Rev. Inorg. Chem.* **1980**, *2*, 253–342.
37. Haiduc, I.; Sowerby, D.B. Stereochemical aspects of phosphor-1,1-dithiolato metal complexes: Coordination patterns, molecular structures and supramolecular associations in dithiophosphinates and related compounds. *Polyhedron* **1996**, *15*, 2469–2521. [CrossRef]
38. Tiekink, E.R.T. Supramolecular association via Hg···S secondary-bonding interactions in crystals of organomercury(II) species: A survey of the Cambridge Structure Database. *Crystals* **2023**, *13*, 385. [CrossRef]
39. Gomila, R.M.; Frontera, A.; Tiekink, E.R.T. Supramolecular aggregation featuring Hg···S secondary-bonding interactions in crystals of mercury(II) species augmented by computational chemistry calculations. *CrystEngComm* **2023**, *25*, 5262–5285. [CrossRef]
40. Iwasaki, H. The crystal structures of dimeric and monoclinic forms of mercury(II) N,N-diethyldithiocarbamate, Hg2(S2CNEt2)4 and Hg(S2CNEt2)2. *Acta Crystallogr. Sect. B Struct. Sci. Cryst. Eng. Mater.* **1973**, *29*, 2115–2124. [CrossRef]
41. Lai, C.S.; Tiekink, E.R.T. Refinement of the crystal structure of bis[(N,N-diethyldithiocarbamato)mercury(II)], [Hg(S2CNEt2)2]2. *Z. Kristallogr.—New Cryst. Struct.* **2002**, *217*, 593–594. [CrossRef]
42. Cox, M.J.; Tiekink, E.R.T. Structural diversity in the mercury(II) bis(N,N-dialkyldithiocarbamate) compounds: An example of the importance of considering crystal structure when rationalising molecular structure. *Z. Kristallogr.—Cryst. Mater.* **1999**, *214*, 571–579. [CrossRef]
43. Cox, M.J.; Tiekink, E.R.T. The crystal structure of monomeric bis(dicyclohexyldithiocarbamato)mercury(II). *Main Group Met. Chem.* **2000**, *23*, 793–794. [CrossRef]
44. Groom, C.R.; Bruno, I.J.; Lightfoot, M.P.; Ward, S.C. The Cambridge Structural Database. *Acta Crystallogr. B Struct. Sci. Cryst. Eng. Mater.* **2016**, *72*, 171–179. [CrossRef] [PubMed]
45. Spek, A.L. checkCIF validation ALERTS: What they mean and how to respond. *Acta Crystallogr. Sect. E Crystallogr. Commun.* **2020**, *76*, 1–11. [CrossRef] [PubMed]
46. Maglic, J.B.; Lavendomme, R. MoloVol: An easy-to-use program for analyzing cavities, volumes and surface areas of chemical structures. *J. Appl. Cryst.* **2022**, *55*, 1033–1044. [CrossRef] [PubMed]
47. Brandenburg, K.; Berndt, M. *DIAMOND*, Version 3.2k; GbR: Bonn, Germany, 2006.
48. Spackman, P.R.; Turner, M.J.; Mckinnon, J.J.; Wolff, S.K.; Grimwood, D.J.; Jayatilaka, D.; Spackman, M.A. CrystalExplorer: A program for Hirshfeld surface analysis, visualization and quantitative analysis of molecular crystals. *J. Appl. Crystallogr.* **2021**, *54*, 1006–1011. [CrossRef]
49. Tan, S.L.; Jotani, M.M.; Tiekink, E.R.T. Utilizing Hirshfeld surface calculations, non-covalent interaction (NCI) plots and the calculation of interaction energies in the analysis of molecular packing. *Acta Crystallogr. Sect. E Crystallogr. Commun.* **2019**, *75*, 308–318. [CrossRef]
50. Ahlrichs, R.; Bär, M.; Häser, M.; Horn, H.; Kölmel, C. Electronic structure calculations on workstation computers: The program-system turbomole. *Chem. Phys. Lett.* **1989**, *162*, 165–169. [CrossRef]
51. Adamo, C.; Barone, V. Toward reliable density functional methods without adjustable parameters: The PBE0 model. *J. Chem. Phys.* **1999**, *110*, 6158–6169. [CrossRef]
52. Grimme, S.; Antony, J.; Ehrlich, S.; Krieg, H. Consistent and accurate ab initio parametrization of density functional dispersion correction (DFT-D) for the 94 elements H-Pu. *J. Chem. Phys.* **2010**, *132*, 154104. [CrossRef]
53. Weigend, F.; Ahlrichs, R. Balanced basis sets of split valence, triple zeta valence and quadruple zeta valence quality for H to Rn: Design and assessment of accuracy. *Phys. Chem. Chem. Phys.* **2005**, *7*, 3297–3305. [CrossRef]
54. Weigend, F. Accurate coulomb-fitting basis sets for H to Rn. *Phys. Chem. Chem. Phys.* **2006**, *8*, 1057–1065. [CrossRef]
55. Bader, R.F.W. A quantum theory of molecular structure and its applications. *Chem. Rev.* **1991**, *91*, 893–928. [CrossRef]

56. Contreras-García, J.; Johnson, E.R.; Keinan, S.; Chaudret, R.; Piquemal, J.-P.; Beratan, D.N.; Yang, W. NCIPLOT: A program for plotting non-covalent interaction regions. *J. Chem. Theory Comput.* **2011**, *7*, 625–632. [CrossRef] [PubMed]
57. Humphrey, W.; Dalke, A.; Schulten, K. VMD: Visual molecular dynamics. *J. Mol. Graph.* **1996**, *14*, 33–38. [CrossRef] [PubMed]
58. Glendening, E.D.; Landis, C.R.; Weinhold, F. NBO 7.0: New vistas in localized and delocalized chemical bonding theory. *J. Comput. Chem.* **2019**, *40*, 2234–2241. [CrossRef]
59. Glendening, E.D.; Badenhoop, J.K.; Reed, A.E.; Carpenter, J.E.; Bohmann, J.A.; Morales, C.M.; Karafiloglou, P.; Landis, C.R.; Weinhold, F. *NBO 7.0*; Theoretical Chemistry Institute, University of Wisconsin: Madison, WI, USA, 2018.
60. Kitaura, K.; Morokuma, K. A new energy decomposition scheme for molecular interactions within the Hartree-Fock approximation. *Int. J. Quantum Chem.* **1976**, *10*, 325–340. [CrossRef]
61. Grdenić, D. The structural chemistry of mercury. *Q. Rev. Chem. Soc.* **1965**, *19*, 303–328. [CrossRef]
62. Lobana, T.S. Coordination chemistry of organomercury(II) involving phenanthrolines, bipyridines, tertiary phosphines/arsines and some related ligands. *Coord. Chem. Rev.* **1985**, *63*, 161–215. [CrossRef]
63. House, D.A.; Robinson, W.T.; McKee, V. Chloromercury(II) anions. *Coord. Chem. Rev.* **1994**, *135–136*, 533–586. [CrossRef]
64. Morsali, A.; Masoomi, M.Y. Structures and properties of mercury(II) coordination polymers. *Coord. Chem. Rev.* **2009**, *253*, 1882–1905. [CrossRef]
65. Schmidbaur, H.; Schier, A. Mercurophilic interactions. *Organometallics* **2015**, *34*, 2048–2066. [CrossRef]
66. Sarker, J.C.; Hogarth, G. Dithiocarbamate complexes as single source precursors to nanoscale binary, ternary and quaternary metal sulfides. *Chem. Rev.* **2021**, *121*, 6057–6123. [CrossRef]
67. Rodina, T.A.; Loseva, O.V.; Smolentsev, A.I.; Antzutkin, O.N.; Ivanov, A.V. Crystal structure, solid-state ^{13}C and ^{15}N NMR characterisation, chemisorption activity and thermal behaviour of new mercury(II) dipropyldithiocarbamate: Binuclear, pseudo-binuclear and heteronuclear complexes of $[Hg_2(PrDtc)_4]$, $[Hg(PrDtc)_2]_2$ and $[Au(PrDtc)_2]_2[Hg_2Cl_6]$. *Inorg. Chim. Acta* **2020**, *508*, 119630. [CrossRef]
68. Loseva, O.V.; Rodina, T.A.; Smolentsev, A.I.; Ivanov, A.V. A new polymorphic modification and chemisorption activity of mercury(II) N,N-di-iso-propyldithiocarbamate: Synthesis and characterisation of the heteronuclear double complex of $([Au\{S_2CN(iso\text{-}C_3H_7)_2\}_2]_2[Hg_2Cl_6]\cdot OC(CH_3)_2)_n$. *Polyhedron* **2017**, *134*, 238–245. [CrossRef]
69. Gomathi, G.; Dar, S.H.; Thirumaran, S.; Ciattini, S.; Selvanayagam, S. Bis(N-benzyl-N-furfuryldithiocarbamato-S,S′)mercury(II) as a precursor for the preparation of mercury sulfide nanoparticles. *C. R. Chim.* **2015**, *18*, 499–510. [CrossRef]
70. Onwudiwe, D.C.; Ajibade, P.A. Synthesis, characterization and thermal studies of Zn(II), Cd(II) and Hg(II) complexes of N-methyl-N-phenyldithiocarbamate: The single crystal structure of $[(C_6H_5)(CH_3)NCS_2]_4Hg_2$. *Int. J. Mol. Sci.* **2011**, *12*, 1964–1978. [CrossRef] [PubMed]
71. Green, M.; Prince, P.; Gardener, M.; Steed, J. Mercury(II) N,N′-methyl-phenylethyl-dithiocarbamate and its use as a precursor for the room-temperature solution deposition of β-HgS thin films. *Adv. Mater.* **2004**, *16*, 994–996. [CrossRef]
72. Onwudiwe, D.C.; Ajibade, P.A. Synthesis and crystal structure of bis(N-alkyl-N-phenyl dithiocarbamato)mercury(II). *J. Chem. Crystallogr.* **2011**, *41*, 980–985. [CrossRef]
73. Ajibade, P.A.; Onwudiwe, D.C. Synthesis and characterization of group 12 complexes of N,N-methylphenyl-N,N-butyl phenyl dithiocarbamate. *J.Coord. Chem.* **2011**, *63*, 2964–2973. [CrossRef]
74. Ondrušová, D.; Pajtášová, M.; Jóna, E.; Koman, M. Structural properties of Co(III), Hg(II) and Pb(II) N-ethyl-N-phenyl-dithiocarbamates and their application in the rubber industry. *Solid State Phenom.* **2003**, *90–91*, 383–388. [CrossRef]
75. Gurumoorthy, G.; Thirumaran, S.; Ciattini, S. Unusual octahedral Hg(II) dithiocarbamate: Synthesis, spectral and structural studies on Hg(II) complexes with pyrrole based dithiocarbamates and their utility for the preparation of α- and β-HgS. *Polyhedron* **2016**, *118*, 143–153. [CrossRef]
76. Guzmán-Percástegui, E.; Zakharov, L.N.; Alvarado-Rodríguez, J.G.; Carnes, M.E.; Johnson, D.W. Synthesis of a self-assembled Hg(II)-dithiocarbamate metallomacrocycle. *Cryst. Growth Des.* **2014**, *14*, 2087–2091. [CrossRef]
77. Yadav, R.; Trivedi, M.; Kociok-Köhn, G.; Chauhan, R.; Kumar, A.; Gosavi, S.W. Ferrocenyl dithiocarbamate based d^{10} transition-metal complexes as potential co-sensitizers in dye-sensitized solar cells. *Eur. J. Inorg. Chem.* **2016**, *2016*, 1013–1021. [CrossRef]
78. Dar, S.H.; Thirumaran, S.; Selvanayagam, S. Synthesis, spectral and X-ray structural studies on Hg(II) dithiocarbamate complexes: A new precursor for HgS nanoparticles. *Polyhedron* **2015**, *96*, 16–24. [CrossRef]
79. Kumar, V.; Manar, K.K.; Gupta, A.N.; Singh, V.; Drew, M.G.B.; Singh, N. Impact of ferrocenyl and pyridyl groups attached to dithiocarbamate moieties on crystal structures and luminescent characteristics of group 12 metal complexes. *J. Organomet. Chem.* **2016**, *820*, 62–69. [CrossRef]
80. Altaf, M.; Stoeckli-Evans, H.; Batool, S.S.; Isab, A.A.; Ahmad, S.; Saleem, M.; Awan, S.A.; Shaheen, M.A. Mercury(II) complexes of pyrrolidinedithiocarbamate, crystal structure of bis{[μ_2-(pyrrolidinedithiocarbamato-S,S′)(pyrrolidinedithiocarbamato-S,S′)mercury(II)]}. *J. Coord. Chem.* **2010**, *63*, 1176–1185. [CrossRef]
81. Loseva, O.V.; Rodina, T.A.; Antzutkin, O.N.; Ivanov, A.V. Chemisorption activity of mercury(II) cyclopentamethylenedithiocarbamate: Synthesis, structure, and thermal behavior of the $[Hg_2\{S_2CN(CH_2)_5\}_4]$ and $[Au_3\{S_2CN(CH_2)_5\}_6][Au\{S_2CN(CH_2)_5\}_2][Hg_2Cl_6]_2$ complexes. *Russ. J. Gen. Chem.* **2018**, *88*, 2540–2549. [CrossRef]
82. Ivanov, A.V.; Korneeva, E.V.; Bukvetskii, B.V.; Goryan, A.S.; Antsutkin, O.N.; Forshling, W. Structural organization of mercury(II) and copper(II) dithiocarbamates from EPR and ^{13}C and ^{15}N MAS NMR spectra and X-ray diffraction analysis. *Russ. J. Coord. Chem.* **2008**, *34*, 59–69. [CrossRef]

83. Benedetti, A.; Fabretti, A.C.; Preti, C. Structure, IR, and NMR spectra of tetrakis(4-methyl piperidinedithiocarbamate) dimercury(II). *J. Crystallogr. Spectrosc. Res.* **1988**, *18*, 685–692. [CrossRef]
84. Khan, A.; Hayat, F.; Butler, I.S.; Tahir, M.N.; ur Rehman, Z. Mercury(II) dithiocarbamates: Structural aspects and their use as single-source precursors for shape-controlled facile synthesis of HgS nanoparticles. *Polyhedron* **2021**, *193*, 114876. [CrossRef]
85. Srinivasan, N.; Thirumaran, S.; Ciattini, S. Effect of co-crystallization of ethanol, pyridine and 2,2′-bipyridine on molecular aggregation in bis(1,2,3,4-tetrahydroquinolinedithiocarbamato-S,S′)mercury(II) and synthesis of HgS nanoparticles. *RSC Adv.* **2014**, *4*, 22971–22979. [CrossRef]
86. Onwudiwe, D.C.; Ajibade, P.A. Synthesis and characterization of Zn(II), Cd(II), and Hg(II) alkyl-aryl dithiocarbamate: X-ray crystal structure of $[(C_6H_5N(et)CS_2)Hg(C_6H_5N(butyl)CS_2)]$. *Synth. React. Inorg. Met.-Org. Nano-Met. Chem.* **2010**, *40*, 279–284. [CrossRef]
87. Marimuthu, G.; Ramalingam, K.; Rizzoli, C.; Arivanandhan, M. Solvothermal preparation of nano-β-HgS from a precursor, bis(dibenzyldithiocarbamato)mercury(II). *J. Nanopart. Res.* **2012**, *14*, 710. [CrossRef]
88. Yadav, M.K.; Rajput, G.; Gupta, A.N.; Kumar, V.; Drew, M.G.B.; Singh, N. Exploring the coordinative behaviour and molecular architecture of new PhHg(II)/Hg(II) dithiocarbamate complexes. *Inorg. Chim. Acta* **2014**, *421*, 210–217. [CrossRef]
89. Kumar, A.; Chauhan, R.; Molloy, K.C.; Kociok-Köhn, G.; Bahadur, L.; Singh, N. Synthesis, structure and light-harvesting properties of some new transition-metal dithiocarbamates involving ferrocene. *Chem.-Eur. J.* **2010**, *16*, 4307–4314. [CrossRef]
90. Marimuthu, G.; Ramalingam, K.; Rizzoli, C. Predominant ionic interactions in CdS_4N_2 and HgS_4 coordination environments. *J. Coord. Chem.* **2013**, *66*, 699–711. [CrossRef]
91. Ito, M.; Iwasaki, H. The structure of the monomeric form of mercury(II) N,N-diisopropyldithiocarbamate [bis(N,N-diisopropyldithiocarbamato)mercury(II)]. *Acta Crystallogr. B* **1979**, *35*, 2720–2721. [CrossRef]
92. Angeloski, A.; Rawal, A.; Bhadbhade, M.; Hook, J.M.; Schurko, R.W.; McDonagh, A.M. An unusual mercury(II) diisopropyldithiocarbamate coordination polymer. *Cryst. Growth Des.* **2019**, *19*, 1125–1133. [CrossRef]
93. Singh, R.P.; Maurya, V.K.; Maiti, B.; Siddiqui, K.A.; Prasad, L.B. Synthesis, structure and thermogravimetric analysis of novel dithiocarbamate based Zn(II),Cd(II) and Hg(II) complexes. *J. Molec. Struct.* **2019**, *1198*, 126912. [CrossRef]
94. Rajput, G.; Yadav, M.K.; Thakur, T.S.; Drew, M.G.B.; Singh, N. Versatile coordination environment and interplay of metal assisted secondary interactions in the organization of supramolecular motifs in new Hg(II)/PhHg(II) dithiolates. *Polyhedron* **2014**, *69*, 225–233. [CrossRef]
95. Lai, C.S.; Tiekink, E.R.T. Crystallographic report: Bis(pyrrolinedithiocarbamato)mercury(II). *Appl. Organomet. Chem.* **2003**, *17*, 143. [CrossRef]
96. Oladipo, S.D.; Omondi, B. *N*,*N*′-diarylformamidine dithiocarbamates as single-source precursors for the preparation of oleylamine-capped HgS nanoparticles. *Transit. Met. Chem.* **2020**, *45*, 391–402. [CrossRef]
97. Singh, V.; Kumar, V.; Gupta, A.N.; Drew, M.G.B.; Singh, N. Effect of pyridyl substituents leading to the formation of green luminescent mercury(II) coordination polymers, zinc(II) dimers and a monomer. *New J. Chem.* **2014**, *38*, 3737–3748. [CrossRef]
98. Healy, P.C.; White, A.H. Crystal structure of bis(NN-diethyldithiocarbamato)mercury(II). *J. Chem. Soc. Dalton Trans.* **1973**, 284–287. [CrossRef]
99. Howie, R.A.; Tiekink, E.R.T.; Wardell, J.L.; Wardell, S.M.S.V. Complementary Supramolecular Aggregation via O–H···O Hydrogen-bonding and Hg···S Interactions in Bis[N,N′-di(2-hydroxyethyl)-dithiocarbamato-S,S′]mercury(II): $Hg[S_2CN(CH_2CH_2OH)_2]_2$. *J. Chem. Crystallogr.* **2009**, *39*, 293–298. [CrossRef]
100. Singh, V.; Kumar, A.; Prasad, R.; Rajput, G.; Drew, M.G.B.; Singh, N. The interplay of secondary Hg···S, Hg···N and Hg···π bonding interactions in supramolecular structures of phenylmercury(II) dithiocarbamates. *CrystEngComm* **2011**, *13*, 6817–6826. [CrossRef]
101. Loseva, O.V.; Rodina, T.A.; Ivanov, A.V. Pseudo-polymeric mercury(II) morpholinedithiocarbamate $[Hg\{S_2CN(CH_2)_4O\}_2]_n$: Supramolecular structure (a role of secondary Hg···S Bonds), ^{13}C and ^{15}N CP-MAS NMR Spectra, and thermal behavior. *Coord. Chem.* **2019**, *45*, 22–29. [CrossRef]
102. Cox, M.J.; Tiekink, E.R.T. Structural variations in the mercury(II) bis(1,1-dithiolate)s: The crystal and molecular structure of $[Hg(S_2CNMe_2)_2]$. *Z. Kristallogr. Cryst. Mater.* **2010**, *212*, 542–544. [CrossRef]
103. Chieh, C.; Cheung, S.K. A crystallographic and spectroscopic study of mercury(II) dithiocarbamate. *Can. J. Chem.* **1981**, *59*, 2746–2749. [CrossRef]
104. Konarev, D.V.; Khasanov, S.S.; Lopatin, D.V.; Rodaev, V.V.; Lyubovskaya, R.N. Fullerene complexes with divalent metal dithiocarbamates: Structures, magnetic properties, and photoconductivity. *Russ. Chem. Bull.* **2007**, *56*, 2145–2161. [CrossRef]
105. Ajibade, P.A.; Mbese, J.Z.; Omondi, B. Group 12 dithiocarbamate complexes: Synthesis, characterization, and X-ray crystal structures of Zn (II) and Hg (II) complexes and their use as precursors for metal sulfide nanoparticles. *Inorg. Nano-Met. Chem.* **2017**, *47*, 202–212. [CrossRef]
106. Moulton, B.; Zaworotko, M.J. From molecules to crystal engineering: Supramolecular isomerism and polymorphism in network solids. *Chem. Rev.* **2001**, *101*, 1629–1658. [CrossRef] [PubMed]
107. Zhang, J.-P.; Huang, X.-C.; Chen, X.-M. Supramolecular isomerism in coordination polymers. *Chem. Soc. Rev.* **2009**, *38*, 2385–2396. [CrossRef]
108. Tan, Y.S.; Halim, S.N.A.; Tiekink, E.R.T. Exploring the crystallization landscape of cadmium bis(N-hydroxyethyl, N-isopropyldithiocarbamate), $Cd[S_2CN(iPr)CH_2CH_2OH]_2$. *Z. Kristallogr.* **2016**, *231*, 113–126. [CrossRef]

109. Addison, A.W.; Rao, T.N.; Reedijk, J.; van Rijn, J.; Verschoor, C.C. Synthesis, structure, and spectroscopic properties of copper(II) compounds containing nitrogen–sulphur donor ligands; the crystal and molecular structure of aqua[1,7-bis(N-methylbenzimidazol-2′-yl)-2,6-dithiaheptane]copper(II) perchlorate. *J. Chem. Soc. Daltons Trans.* **1984**, 1349–1356. [CrossRef]
110. Yang, L.; Powell, D.R.; Houser, R.P. Structural variation in copper(I) complexes with pyridylmethylamide ligands: Structural analysis with a new four-coordinate geometry index, τ4. *Dalton Trans.* **2007**, 955–964. [CrossRef]
111. Grimme, S.; Mück-Lichtenfeld, C.; Erker, G.; Kehr, G.; Wang, H.; Beckers, H.; Willner, H. When do interacting atoms form a chemical bond? Spectroscopic measurements and theoretical analyses of dideuteriophenanthrene. *Angew. Chem. Int. Ed.* **2009**, *48*, 2592–2595. [CrossRef]
112. Foroutan-Nejad, C.; Shahbazian, S.; Marek, R. Toward a consistent interpretation of the QTAIM: Tortuous link between chemical bonds, interactions, and bond/line paths. *Chem.–Eur. J.* **2014**, *20*, 10140–10152. [CrossRef]
113. Spackman, M.A. How reliable are intermolecular interaction energies estimated from topological analysis of experimental electron densities? *Cryst. Growth Des.* **2015**, *15*, 5624–5628. [CrossRef]
114. Wick, C.R.; Clark, T. On bond-critical points in QTAIM and weak interactions. *J. Mol. Model.* **2018**, *31*, 142. [CrossRef]
115. Scheiner, S. Quantum chemical analysis of noncovalent bonds within crystals. Concepts and concerns. *CrystEngComm* **2023**, *25*, 5060–5071. [CrossRef]
116. Tiekink, E.R.T. Supramolecular assembly based on "emerging" intermolecular interactions of particular interest to coordination chemists. *Coord. Chem. Rev.* **2017**, *345*, 209–228. [CrossRef]
117. Alvarez, S. A cartography of the van der Waals territories. *Dalton Trans.* **2013**, *42*, 8617–8636. [CrossRef]
118. Hu, S.-Z.; Zhou, Z.-H.; Xie, Z.-X.; Robertson, B.E. A comparative study of crystallographic van der Waals radii. *Z. Kristallogr.—Cryst. Mater.* **2014**, *229*, 517–523. [CrossRef]
119. Balmohammadi, Y.; Khavasi, H.R.; Naghavi, S.S. Existence of untypical halogen-involving interactions in crystal packings: A statistical and first-principles study. *CrystEngComm* **2020**, *22*, 2756–2765. [CrossRef]
120. Politzer, P.; Murray, J.S. The use and misuse of van der Waals radii. *Struct. Chem.* **2021**, *32*, 623–629. [CrossRef]